Original Research Communication

Title: A new class of thioredoxin-related protein able to bind iron-sulfur clusters

Author affiliation: Hugo Bisio[a], Mariana Bonilla[b], Bruno Manta[b], Martín Graña[c], Valentina Salzman[d], Pablo S Aguilar[d], Vadim N Gladyshev[e], Marcelo Comini[b] and Gustavo Salinas[a,f].

[a] Worm Biology Laboratory, Institut Pasteur de Montevideo. Montevideo, Uruguay.

[b] Redox Biology of Trypanosomes Laboratory, Institut Pasteur de Montevideo. Montevideo, Uruguay.

[c] Bioinformatics Unit, Institut Pasteur Montevideo de. Montevideo, Uruguay.

[d] Cellular Membranes Laboratory, Institut Pasteur de Montevideo. Montevideo, Uruguay.

[e] Division of Genetics, Department of Medicine, Brigham & Women's Hospital and Harvard Medical School. Boston, USA.

[f] Cátedra de Inmunología, Departamento de Biociencias, Facultad de Química, Universidad de la República. Montevideo, Uruguay.

Corresponding Author: Gustavo Salinas

Worm Biology Laboratory, Institut Pasteur de Montevideo. Mataojo 2020, Montevideo 11400, Uruguay. Telephone number: +598 25220910 ext 179. E-mail: gsalin@fq.edu.uy

Keywords: thioredoxin, iron-sulfur, glutaredoxin, iron metabolism, thioredoxin-fold, iron-sulfur metabolism, Echinococcus.

Abstract

***Aims*:** Members of the thioredoxin (Trx) protein family participate mainly in redox pathways and have not been associated with Fe/S binding, in contrast to some closely related glutaredoxins (Grxs). Cestode parasites possess an unusual diversity of Trxs and Trx-related proteins with non-explored functions. Here we addressed the biochemical characterization of a new class of Trx-related protein (IsTRP) and a classical monothiol Grx (EgGrx5) from the human pathogen *Echinococcus granulosus*. ***Results*:** The dimeric form of IsTRP coordinates Fe_2S_2 in a glutathione-independent manner; instead, Fe/S binding relies on the CXXC motif conserved among Trxs. This novel binding mechanism allows holo-IsTRP to be highly resistant to oxidation. IsTRP lacks canonical reductase activities. Mitochondrially targeted IsTRP aids growth of a Grx5 null yeast strain. Similar complementation assays performed with EgGrx5 revealed functional conservation for class II Grxs despite the presence of non-conserved structural elements. IsTRP is a cestode-lineage specific protein highly expressed in the gravid adult worm, which releases the infective stage critical for dissemination. ***Innovation*:** IsTRP is the first member from the thioredoxin family to be reported to bind Fe/S. We disclose a novel mechanism of Fe/S coordination within the Trx folding unit, which renders the cluster highly resistant to oxidation-mediated disassembly. ***Conclusion*:** We demonstrate that IsTRP defines a new protein family within the thioredoxin superfamily, confirm the conservation of function for class II glutaredoxin from non-phylogenetically related species and highlight the versatility of the Trx folding unit to acquire Fe/S binding as a recurrent emergent function.

Introduction

The thioredoxin (Trx) superfamily includes a wide range of proteins with diverse functions that shares a common structural pattern, the thioredoxin fold unit, composed of a β-sheet consisting of four beta strands, surrounded by three α-helices (35). The prototypical Trx is a thiol-dependent oxidoreductase with a characteristic WCGPC dithiol active site motif that functions mainly as protein disulfide reductase (16). Thioredoxin reductase (TR) maintains Trxs in their reduced form (19, 33) at the expense of NADPH oxidation. Trx-related proteins (TRP) or Trx-like proteins also possess a Trx-fold with a canonical Trx active site and are involved in redox homeostasis (34). Glutaredoxins (Grxs), which utilize glutathione (GSH) as cofactor for their functions, also belong to the Trx superfamily (26). Grxs are clustered into three classes (44), with classes I and II being widely distributed. Class I Grxs possess a canonical CPYC active site and their main functions rely on their redox activity, particularly as protein disulfide and GSH-protein disulfide reductases, involved in an oxidoreduction cascade with GSH, glutathione reductase (GR) and NADPH (33). On the other hand, class II Grxs possess a typical CGFS active site and are functionally distinct: they exhibit low or no thiol-disulfide oxidoreductase activity (14, 21, 47, 53) and their main role relate to iron homeostasis (24). Mitochondrial class II Grxs, such as *Saccharomyces cerevisiae* Grx5 (ScGrx5), are usually indispensable components of the mitochondrial iron sulfur cluster assembly machinery (ISC), participating in Fe/S trafficking and assembly to apoproteins (24, 37). Fe/S are essential cofactors for oxidative phosphorylation, some Krebs cycle enzymes, protein synthesis, among other important pathways. These requirements

provide the basis for assessing the function of Grx5 (23). The ISC includes several proteins and is essential for Fe/S synthesis in the mitochondria and, most likely, in the cytosol (24). The dependence to the mitochondria for *de novo* synthesis in the cytosol is controversial (38) but the most accepted view emphasizes that Fe/S synthesis starts in the mitochondria from which a sulfur-containing moiety is exported to the cytosol, in a process dependent of an ABC transporter and GSH, but details are not fully understood (43). In mammals, the presence of cytosolic and nuclear forms of some components of the ISC has raised the possibility that Fe/S could be synthesized *de novo* in these compartments (38). In any case, the cytosolic Fe/S protein assembly machinery (CIA) is necessary for further processing the Fe/S in the cytosol (23). Finally, class III Grxs are restricted to angiosperms, possess a CC(M/L)(C/S) active site sequence and represent the large majority of the Grxs encoded in higher plants genomes. These proteins seem to be involved in the resistance of plants to a variety of different environmental conditions (44).

Generally speaking, Trx-fold proteins mainly serve as thiol/disulfide oxidoreductases and only a small subset binds metal ions (46). Class II and some class I Grxs bind Fe/S in a dimeric fashion, where the iron atoms of the cluster are coordinated by the N-terminal active site cysteine residue (Cys) of each subunit and by two non-covalently bound GSH molecules (4). Different types of Fe/S have been shown to be bound to Grxs, including rhombic $[Fe_2S_2]^{2+}$, linear $[Fe_3S_4]^{+}$ and $[Fe_4S_4]^{2+}$ (54). In addition to this canonical binding through GSH, an unusual mode of Fe/S coordination was reported in Grx2 from the teleost fish (8). The monomeric form of this protein can bind Fe/S using four Cys residues different from the CxxC active site. Trx-like ferredoxins (52) are also able to bind Fe/S. This type of ferredoxins forms homodimers bound by protein/protein

interactions in which each subunit coordinates one [Fe_2S_2] through four Cys residues (29, 52). Although the function of these proteins is still unclear, they might be involved in nitrogen fixation, since it has been shown that they interact with a molybdenum-containing nitrogenase (15, 29). Finally, TrxA from *Escherichia coli* (27) and human Trx1 (46) are able to coordinate Fe/S when specific non-natural mutations are introduced in their sequences.

Parasitic tapeworm genomes have revealed an unexpected diversity of Trxs and Grxs (5, 49), but the functions of most of these proteins have not been examined. This diversity contrasts with the minimalistic arrangement of the upstream pathway, where GR and TR have been replaced by a single enzyme, the thioredoxin glutathione reductase (TGR), which provides electrons to Trxs and Grxs at expenses of NADPH (51).

Here we characterized an ortholog of yeast Grx5 in the tapeworm *Echinococcus granulosus* (Grx5), and a new Trx-fold protein, which we designate Iron-sulfur Trx-related protein (IsTRP) that is the first wild type Trx-like protein with Fe/S coordination capacity to be reported. We show that its Fe/S binding is GSH-independent, involves dimerization, and uses two Cys residues from each monomer as ligands for iron coordination of the cluster. A model for the relevance of IsTRP for Fe/S supply during infection of the intermediate host is proposed.

Results

Common and unique features of cestode IsTRP and Grx5.

IsTRP possesses a Trx-like domain, which unequivocally clusters with Trxs and Trx-related proteins in the phylogenetic analysis, and is distant to all other Trx-fold proteins (Fig. 1A). A conspicuous feature of IsTRP is the presence of an additional Cys residue immediately adjacent to the canonical active site CxxC motif, resulting in the CxxCC motif. Data mining of orthologous genes showed that IsTRP is encoded exclusively by the *Cyclophyllidea* order within the class *Cestoda* and is absent in any other sequenced lineage. Interestingly, the third Cys is conserved in most, but not all IsTRPs (Fig. 1B). None of the cestode IsTRPs has a sorting signal peptide. Since there are no RNASeq data of IsTRP in *E. granulosus*, we examined the expression data from *Echinococcus multilocularis,* kindly provided by Dr. Matt Berriman. This data mining indicated that IsTRP is highly expressed in the gravid adult (the stage that releases embryonated eggs to the environment) while very low expression is observed in other stages of the parasite (Fig. S1). In contrast, Grx5 is a highly conserved mitochondrial class II Grx, with orthologous proteins present in a wide range of eukaryotic lineages. A remarkable feature of parasitic flatworms Grx5 is that they possess a unique insertion of 8 amino acids in an infrequent insertion site in the Trx superfamily, located between the active site containing α-helix and the following β-strand (Fig. 1C). Analysis of a homology-based model of *E. granulosus* Grx5 indicates that this element does not impose any significant constrain to the Trx domain folding core (Fig. S2). Interestingly, this insertion defines an extended loop located near the class II Grx acidic surface that

is proposed to be important for the interaction with its partners (21). Grx5 from parasitic flatworms also harbor a non-conserved cysteine residue at the C-terminus of the α-helix containing the active site.

Dimeric IsTRP and Grx5 coordinate Fe/S.

IsTRP and Grx5 were expressed as His-tagged recombinant proteins in *E. coli* and affinity purified as a brownish solution with UV-visible spectra compatible with the presence of bound Fe/S. Size exclusion chromatography (SEC) of purified proteins revealed a mixture of monomeric and dimeric forms for both proteins (Fig. 2A and 2C). IsTRP eluted with an apparent molecular mass of 22 and 11 kDa, corresponding to the dimeric and monomeric forms, respectively (theoretical mass of the monomer 15.6 kDa). In the case of Grx5, the protein eluted with an apparent molecular mass of 54 and 35 kDa, likely corresponding to the dimer and monomer even though the theoretical mass of the monomer is 20.2 kDa. This shift in the apparent molecular mass of Grx5 is probably consequence of an increased radius due to a flexible N-terminal extension present in the recombinant protein (see full sequence in Fig. S3). The fractions containing the dimers for IsTRP and Grx5, but not those containing the monomers, displayed absorbance at 320 and 420 nm (Fig 2A and 2C) and a UV-visible spectra (Fig 2B and D) similar to Fe/S binding proteins (4, 54), suggesting Fe/S binding. Furthermore, the formation of dimers was dependent on cluster binding since EDTA treatment (Fig. 2A and 2B) decreased the dimer/monomer ratio. Moreover, in vitro reconstitution of Fe/S (Fig. 2E and 2F) increased the dimer/monomer ratio.

IsTRP coordinates 2Fe2S clusters.

The UV-visible spectrum of holo-IsTRP suggested the presence of a 2Fe2S in the cluster bound by this protein. In order to confirm the nature and the stoichiometry of the

cluster in holo-IsTRP obtained *in vivo* from *E. coli*, the iron and sulfur content was assessed using analytical techniques (Table 1). Iron was measured with 4,7-diphenyl-1,10-phenanthroline and by atomic absorption, and sulfide was measured by the methylene blue technique. The results were consistent with the presence of one 2Fe2S center per dimer.

Fe/S coordination by IsTRP is stable, dependent on two Cys residues of the polypeptide chain and GSH independent.

In order to characterize Fe/S binding by IsTRP, absorbance of the holocomplex was followed over time in presence or absence of GSH and/or H_2O_2 (Fig. 3A). Experiments with Grx5 were carried out in parallel for comparison (Fig 3B). Interestingly, GSH did not increase stability of the Fe/S bound to IsTRP, in contrast to Fe/S coordinated by Grx5. Also, the IsTRP-bound Fe/S was far more stable (fifty-fold) to H_2O_2 treatment than that bound by Grx5, even when GSH was present in the Grx5 assay mixture (data not shown). We next examined the importance of IsTRP Cys residues in Fe/S binding using Cys→Ser mutants of each Cys residue (i.e., SxxCC, CxxSC and CxxCS). Fe/S coordination by wild type and mutant proteins was further assessed by a spectrophotometric analysis of recombinant proteins (Fig. 3C and 3D). Two cysteine residues, Cys 34 and Cys 37, corresponding to nucleophilic and resolving positions of catalytic cysteines in Trxs, respectively, were found to be essential for cluster binding by IsTRP since the 320/280 nm absorbance ratios of these mutants were 15% and 8% of the wild-type protein ratio. Also, these mutants displayed mostly a monomeric behavior when analyzed by size exclusion chromatography (data not shown). In contrast, the contiguous Cys 38 was not required for Fe/S binding by IsTRP. These data, the lack of a stabilizing effect of GSH on holo-IsTRP and the absence of the

characteristic GSH-binding site residues in the sequence, strongly support that IsTRP binds Fe/S by a GSH-independent mechanism. To further test this model, the holo and apo protein fractions of IsTRP and Grx5 obtained from *E. coli* were acid-precipitated and total low molecular weight thiols and GSH were measured (Table 2). The results indicated that neither GSH nor any other low molecular weight thiol was an integral component of the holo-IsTRP, while, as previously reported for canonical Fe/S Grxs (4), GSH was found as a cofactor for the holo-Grx5.

IsTRP did not exhibit canonical reductase activities.

The disulfide redox activity of the recombinant IsTRP and Grx5 were tested using the insulin (17) and HED (18) reduction assays; a canonical *E. granulosus* Trx (EUB56960.1) (7) and Grx (CDS21744.1) were used as positive controls. The apo- and holo- forms of IsTRP and apo-Grx5 were unable to efficiently catalyze the reduction of these substrates under the reaction conditions tested (Fig. 4A and 4B). A marginal catalytic activity in the HED assay by Grx5 was observed. Also, it is worth mentioning that the oxidized apo-IsTRP was reduced by TGR (AAN63052) in a NADPH-dependent assay, but only at high TGR concentration (Fig. 4C). The Cys 34 and Cys 37 residues contributed to disulfide formation, since the corresponding Ser mutants showed a significant reduction in NADPH consumption by TGR. In particular, mutation of Cys 34, corresponding to the nucleophilic Cys in Trxs, led to a complete loss of TGR reductase activity with this substrate, indicating that this residue is involved in the disulfide formation. In order to test if IsTRP could catalyze the reduction of specific targets, pull down experiments were performed using the CxxS mutant. This strategy has proved to be very efficient, particularly for identifying targets of Trxs and Grxs in different organisms (e.g. (45)). We examined protein extracts from the larval stage of *E.*

granulosus (protoscolex) and gravid adult worms (the stage where IsTRP is highly expressed) from the closely related parasite *Hymenolepis microstoma* (an experimental model non-infective to humans (12)). No specific targets were trapped: the same proteins were identified in the CxxS mutant, wild-type and buffer control samples. Finally, we tested whether IsTRP possesses ferredoxin activity in the cytochrome c reduction assay *in vitro*. No ferredoxin activity was detected for IsTRP, a spinach ferredoxin was used as a positive control (data not shown).

Grx5 and IsTRP can rescue the *S. cerevisiae* Grx5-deficient yeast phenotype.

We tested whether the *E. granulosus* Grx5 replaces the canonical yeast mitochondrial class II Grx (Grx5). As IsTRP belongs to the same protein superfamily as mitochondrial class II Grxs and both are able to coordinate Fe/S, we also examined whether IsTRP can replace *S. cerevisiae* Grx5. We expressed the *E. granulosus* IsTRP and Grx5 in the mitochondria of the *S. cerevisiae* Grx5 null mutant strain (30). This null strain grows slowly in glucose and is unable to grow using glycerol (non-fermentable substrate) as the sole carbon source (30). As shown in Fig. 5A and 5B, the mitochondrial targeted *E. granulosus* Grx5 rescued the growth defects of the mutant lacking Grx5. To a lower extent, the expression of IsTRP also allows growth on glycerol of the Grx5 null yeast strain (Fig 5A and 5B). The aconitase to malate dehydrogenase activity ratios were also measured to assess the efficiency of Fe/S assembly (Fig 5C), confirming the magnitude of the yeast rescued phenotype for both strains.

The Fe/S synthesis pathway genes are encoded in the genome of *Echinococcus granulosus* and are controlled at the transcriptional level.

Since Fe/S synthesis in platyhelminthes has not been characterized yet, we examined the presence of the known key genes involved in mitochondrial and cytosolic iron

sulfur protein assembly machineries (ISC and CIA, respectively) in *E. granulosus* and *E. multilocularis* (a close related species with a similar life cycle) genomes. This survey indicated that complete ISC and CIA machineries are present in these organisms. Furthermore, the RNAseq data from *E. granulosus* (55) indicated that the genes are actively transcribed during most of the parasite life-cycle, with the exception of activated oncospheres (the newly released embryo in the intermediate host after hatching of the ingested egg), where almost all genes of the CIA Fe/S synthesis pathway and some of the ISC machinery (including Grx5) are completely silenced (Table 3).

Discussion

Parasitic flatworms have been previously shown to possess specific adjustments in their Trx and GSH pathways. Some of the striking features of these pathways were the replacement of conventional TR and GR by TGR and the GSH-independent reduction of glutathionylated proteins by TGR (6). Since Trx and GSH pathways are linked and streamlined in these organisms, the presence of several Trx and Grx genes in tapeworm genomes is also intriguing (49). In the current study, we identified and characterized two Trx-fold proteins of the tapeworm *E. granulosus*: a mitochondrial Fe/S-binding Grx5 that possess an unusual extended loop and IsTRP, a novel class of Trx-related protein that bound Fe/S independently of GSH and lacked classical thiol-disulfide oxidoreductase ativity.

Metal coordination by Trx-fold proteins is not a random event since the majority of oxidoreductases within this superfamily undergo sequence and structural modifications to avoid metal binding (46). As shown in this study, IsTRP coordinates Fe/S through the Cys 34 and Cys 37 residues, which correspond to the homologous positions of nucleophilic and resolving Cys of Trxs, respectively. These highly conserved residues in Trxs do not coordinate Fe/S and in fact this binding would be highly disadvantageous for the oxidoreductase activity. In the reduced state, the resolving Cys of Trxs is partially occluded avoiding Fe/S binding and therefore, there must be some adaptations (permanent or induced) on the structure of IsTRP in order to locate the resolving Cys in the correct spatial location to coordinate the Fe/S. The homology model for IsTRP revealed that Cys 37 would be also occluded (Fig. S4). If the model is correct, the

assembly of Fe/S in the apo-IsTRP must induce a conformational change in order to allow Cys 37 to be available for binding. This conformational change could be similar to what has been proposed for the mechanism of *Escherichia coli* TrxA mutant, with a CACA active site that binds Fe/S (27). Upon Fe/S coordination, this protein would form dimers and one of the subunits would display a partial unfolding at the N-terminus of the active site α-helix (11). A similar conformational change may expose Cys 37 and allows this residue to coordinate Fe/S. Future efforts will be directed at gaining further insights into the structural features of IsTRP that allow this protein to replace the canonical oxidoreduction activity of TRPs for Fe/S binding.

Thus, if Fe/S is not a random event and requires structural adjustments of the fold, the coordination capacity of IsTRP is most likely physiologically relevant. A possible function for the Fe/S might be the regulation of the redox activity of the apoprotein, as proposed for class I Grxs (4). However, oxidoreductase activity was not detected in the canonical Trx and Grx assays and we did not succeed in identifying IsTRP targets using the CxxS mutant in pull down experiments. In any case, the high stability of the holocomplex implies that cluster disassembly to render the active form of IsTRP would demand harsh oxidizing conditions or the action of specific stimuli (e.g. protein partners). Alternatively, IsTRP may function as storage for Fe/S. The ability of IsTRP to slightly suppress the phenotype of the Grx5 null mutant yeast would suggest that this protein might be able to incorporate Fe/S in a eukaryotic system and collaborate in Fe/S transfer to other proteins. It should be noted that overexpression of other members of ISC, such as ferredoxin, can partially rescue the Grx5 knock out phenotype (37). The lack of ferredoxin activity of IsTRP ruled out this possibility. Additional experiments need to be performed to obtain conclusive evidence regarding IsTRP

specific function(s). On the other hand, we demonstrated here that *E. granulosus* Grx5 is able to replace Grx5 function in yeasts, despite having an extended loop in a non-canonical insertion site of the Trx fold. This provides further evidence of the functional conservation of mitochondrial class II Grxs among different lineages of life (31). Thus, the structural singularities of *E. granulosus* Grx5 may play a regulatory role or be important for parasite specific functions (*i.e.* interaction with parasite specific partners).

Though Fe/S biosynthesis has not been studied in platyhelminth parasites, all genes involved in this metabolic process are present in these organisms, suggesting that Fe/S are synthesized de novo.Interestingly, the RNASeq data indicate that most of the genes of the Fe/S biosynthesis are silenced in activated oncospheres. The oncosphere is activated by gastrointestinal cues (e.g. pH), penetrates the intestinal wall and migrates through the circulatory system to internal organs (preferentially liver and lung), where it develops as the metacestode larval stage. The decrease in the synthesis of weakly bound Fe/S and the concomitant decrease of the source of free iron and sulfide are likely important during migration and establishment, when the parasite is particularly exposed to the hostile environment imposed by the host. This raises the question of how is Fe/S supplied to newly synthesized essential enzymes (3, 23) during early infection in the intermediate host. We hypothesize that IsTRP might be relevant at this stage as ready to use storage of preformed Fe/S, synthesized during egg generation. Indeed, IsTRP is highly expressed in the gravid adult (while Fe/S is still being synthesized) and the Fe/S bound to IsTRP is resistant to oxidation.

To sum up, this study describes an entirely new class of proteins of the thioredoxin fold unit: a thioredoxin-related protein that lacks classical oxidoreductase activity but can

bind Fe/S by a unique mechanism, involving both Cys from the active site and no glutathione. Overall our results recapitulate some laboratory evolution experiments (27, 45) highlighting the versatility of the Trx folding unit that, in addition to the different adaptations for redox functions, also displays Fe/S binding as a recurrent emergent function.

Innovation

IsTRP defines a new class of a Trx-related protein able to bind Fe/S. We disclose a novel mechanism of Fe/S coordination within the Trx folding unit, which renders the cluster highly resistant to oxidation-mediated disassembly. IsTRP is present exclusively in some flatworm parasites and highly expressed in the gravid adult worm. In addition, we confirm the function of *E. granulosus* Grx5 in mitochondrial Fe/S biosynthesis, despite possessing distinctive parasite-specific features. Our results uncover lineage specific adaptations of the Trx fold and provide a putative pharmacological target for neglected diseases caused by flatworm infections.

Materials and Methods

Bioinformatics analysis. Genomic data was obtained from the Sanger Institute or generic databases. Multiple protein sequences alignments were generated with Clustalw (22). Maximum likelihood and neighbour-joining trees bootstrap values (500 replicates) were calculated using the MEGA 6 package/software (48).

Cloning of *E. granulosus* proteins for bacterial and yeast expression. The ORF of the IsTRP and Grx5 were amplified from cDNA of *E. granulosus* protoscolex total mRNA and cloned into pET28a (Novagen) using standard molecular cloning techniques, thereby introducing an N-terminal His-tag. Mutants of IsTRP were generated by site-directed mutagenesis using the overlap extension method (39). IsTRP and Grx5 constructs for yeast expression were generated by PCR amplification using pET28a constructs as DNA templates and cloned into the pMM221 plasmid (30). All primers and vectors generated are shown in Table S1. Constructs were sequenced in all cases.

Expression and purification of recombinant proteins. The recombinant protein expression was carried out in *E. coli* BL21(DE3) cells following standard protocols. Essentially, recombinant clones were grown on LB in the presence of kanamycin, and induction of recombinant proteins was carried out with 100 µM isopropyl 1-thio-β-D-galactopyranoside at early exponential phase (Abs_{600nm}= 0.6) over night at 25 °C. The bacterial cultures were centrifuged, and the pellets were resuspended in lysis buffer (300 mM NaCl, 50 mM sodium phosphate, 10 mM imidazole, pH 7.2) containing 1 mM phenylmethylsulfonyl fluoride, and sonicated. The lysates were centrifuged for 30 min at 20,000 x g, and supernatants were applied to a HisPur™

Cobalt Superflow Agarose column (Thermo), washed with 300 mM NaCl, 50 mM sodium phosphate, 20 mM imidazole, pH 7.2, and eluted with 250 mM imidazole. When it is specified, 1 mM glutathione (GSH, Sigma) was added during all steps of purification. Protein concentrations were determined spectrophotometrically at 280 nm (ε_{280}= 7575 and 5625 $M^{-1}cm^{-1}$ for IsTRP and Grx5 respectively) and purity was assessed on 15% SDS-polyacrylamide gels, under reducing conditions. TGR_{C31S} was produced and purified as previously described in (7).

Recombinant protein analysis. Protein fractions were subjected to gel chromatography on Superdex 75 10/300 GL column (GE Healthcare), pre-equilibrated in PBS (pH 7.0), coupled to ÄKTA-FPLC system (GE) with online UV–visible detection. Standard globular proteins (6.5–75 kDa; GE kit) were used for the calibration of the columns. Absorbance at 280, 320 and 420 nm was recorded. UV-visible spectra and reducing SDS-PAGE gels were carried out for the purified fractions. For low molecular weight thiol-containing compounds determinations, size exclusion chromatography fractions were subjected to 5% trichloroacetic acid treatment during 30 min on ice for complete Fe/S disassembly, and 20.000 x g centrifugation, for protein removal. Samples were neutralized in all cases. DTNB recycling assay was performed, as previously described (32), for measuring total GSH and the Ellman's reaction was used to measure total free thiols, following manufacturer´s specifications (Thermo). Protein concentration was meassured prior to Fe/S disassembly. Iron determination was done using 4,7-diphenyl-1,10-phenanthroline (Sigma) as previously described (28). Ferric iron was reduced using ascorbic acid (Fisher) and standard curves were performed using ammonium iron (II) sulfate (Aldrich). Sulfur determination was performed as described in (9, 41). Briefly, 150 µL of 20 mM N.N-dimethyl-p-phenylenediamine dissolved in 7.2 N hydrochloric acid and 150 µL of

30 mM ferric chloride in 1.2 N hydrochloric acid were added to a final volume of 1 mL. 1.5 mM zinc acetate was added to the reaction in order to avoid sulfide gas loss. The absorbance at 670 nm was determined after 20 min of incubation. Standard curves were performed using sodium sulfide. The Fe content of IsTRP was determined by atomic absorption using a Plasma Emission Spectrometer (Jarrell-Ash 965 ICP) in Chemical Analysis Laboratory, University of Georgia.

Fe/S reconstitution Assay. Purified IsTRP was treated with thrombin in order to obtain the tag-free protein and afterwards thrombin was removed by a p-aminobenzamidine–Agarose prepacked column (Sigma). In vitro Fe/S reconstitution of IsTRP was performed as described (4). 100-200 µM of IsTRP was incubated under argon atmosphere at room temperature with 10 mM equivalents of *E. coli* cysteine desulfurase IscS, 2.5–5 equivalents of cysteine, 2–4 equivalents of $Fe(NH_4)_2(SO4)_2$, 1 mM GSH, 5 mM DTT and 10 µM pyridoxal phosphate in 50 mM sodium phosphate buffer, pH 8.0, containing 200 mM NaCl.

Expression of IsTRP and Grx5 in Grx5-deficient *S. cerevisiae*. All employed yeast strains belong to the W303 genetic background and are summarized in Table S2. The plasmids were linearized by ClaI digestion and then used for transformation by the standard lithium salts method (1). Crosses between yeast strains, sporulation and tetrad analyses were carried out by standard genetic techniques. *S. cerevisiae* cultures were grown at 30°C in YPD, YPG (as YPD but with 3% glycerol instead of dextrose) or YPGal (as YPD but with 2% galactose instead of dextrose), as previously described (30).

Enzymatic assays. The insulin interchain disulfides reduction was performed as described in (17). The reduction of two interchain disulfides of insulin catalyzed by IsTRP in the presence of DTT was used as a measure of Trx activity. The reaction was

followed by the increase in absorbance at 650 nm due to the precipitation of free insulin β-chain. The 0.8-ml reaction mixtures contained 0.33 mM DTT, 130 µM insulin and 2mM or non EDTA in 100mM potassium phosphate buffer, pH 7.0. Time courses with DTT alone and the reaction catalized by an *E. granulosus* Trx (2 µM, EUB56960.1) were performed as controls. The glutaredoxin assay was performed as described previously (18). A reaction mixture containing 1 mM GSH (Sigma), 2 mM or non EDTA, 0.1 mg ml^{-1} bovine serum albumin, 0.7 mM β-hydroxyethyl disulfide (Acros Organics), and 0.4 units of yeast glutathione reductase (Sigma) was preincubated for 2 min. Afterward, the protein was added and then the reduction of the mixed glutathione-hydroxyethyl disulfide followed by the oxidation of NADPH at 340 nm. Reduction of spontaneously oxidized IsTRP by the TGR_{C31S} mutant (lacking the Grx and glutathione reductase activities) (6) was performed as described in (20). The mixture containing 100 mM potassium phosphate buffer, pH 7.0, 1 mM EDTA, 0.1 mg/ml BSA, 100 µM NADPH, and 20µM IsTRP. The reaction was started by addition of 125 nM of TGR_{C31S}. Aconitase and malate dehydrogenase activities were assayed following the methods described in (36). Ferredoxin activity was determined following the generation of reduce cytochrome C at 550 nm. 0.3 mM NADPH, 50 mM Tris pH 8.5, 50 µM cytochrome c (Sigma) and 47 nM of pea ferredoxin reductase (40). Up to 50 µM IsTRP was added to the assay and 2.5 µM spinach ferredoxin (Sigma) was used as positive control.

Pull down experiments. 1 mg of $IsTRP_{wt}$, $IsTRP_{CxxS}$ mutant or only buffer samples were incubated for 30 min at 4ºC under gentle agitation with Ni-NTA Magnetic Agarose Beads (Qiagen). The immobilized bait was then incubated with aqueous extracts obtained from 100 µL of packed *E. granulosus* protoscolex or *H. microstoma* adult

worms homogenized using a mortar and pestle under liquid nitrogen and sonicated. After washing ten times with 300 mM NaCl, 50 mM sodium phosphate, 30 mM imidazole, pH 7.2, elution was performed with 10 mM DTT and 8 M urea. In-gel trypsin digestion was performed and the samples extracted from the gel were analyzed in a reverse phase EASY-Spray column, 50 cm × 75 µm ID, PepMap RSLC C18, 2 µm, (Thermo Scientific) and a LTQ VELOS nano-ESI (Thermo Scientific). PatternLab for Proteomics (version 3.2.0.3) was used for spectra analysis and protein identification (10).

Homology models generation. Crystal structures were retrieved from the PDB using the HHpred suite for distant homology detection (42). A multiple-template approach was taken using Modeller version 9v11 (50) to build models from the multiple structural alignments gathered by the HHsuite. 3ipzA, 2wulA, 2yanA and 3zywA were used as templates for Grx5. For TRP, the templates were 3m9jA, 2vimA, 4aj8A, 2yoiA and 4i8bA. The best models obtained from 50 iterations were determined with the DOPE method, included in the Modeller suite. Overall quality assessment of the final models was done with Coot (13). Electrostatic calculations were made with the Adaptive Poisson–Boltzmann Solver (2). All figures illustrating protein structure were prepared using open-source PyMOL (http://www.pymol.org/).

Acknowledgements

We thank Dr. Enrique Herrero (Universitat de Lleida, Spain) for provision of yeast strains and helpful experimental assistance, Dr. Matt Berriman (Parasite Genomics, Wellcome Trust Sanger Institute) for provision of data from *Echinococcus multilocularis* transcriptome, Dr. Rosario Durán (Analytical and Biochemical Proteomic Unit, Institut Pasteur Montevideo) for technical assistance with proteomics, Dr. Néstor Carrillo for provision of purified pea ferredoxin and assistance with the ferredoxin assay and Dr. Massimo Bellanda (University of Padova) for helpful discussions. This work was supported by Universidad de la República, Uruguay (Grant Number I+D 625 to G.S. and INI 915 to H.B.), Agencia Nacional de Innovación e Investigación (POS_NAC_2012_1_8789), ICGEB Research Grant URU14-01 to G.S. and M.C, and FOCEM (MERCOSUR Structural Convergence Fund, [COF 03/11]), and Seeding Labs.

Author Disclosure Statement

No competing financial interests exist.

Abbreviations:

CIA: cytosolic iron sulfur protein assembly machinery, DTNB: di-thio nitro benzoic acid, Fe/S: iron sulfur cluster, Grx: glutaredoxin, GSH: glutathione, ISC: mitochondrial iron sulfur cluster assembly machinery, IsTRP: Iron sulfur thioredoxin-related protein, ORF: open reading frame, TGR: thioredoxin glutathione reductase, TRP: thioredoxin-related protein, Trx: thioredoxin.

References

1. Agatep R. Transformation of *Saccharomyces cerevisiae* by the lithium acetate/single-stranded carrier DNA/polyethylene glycol protocol. *Technical Tips Online* 3, 133–137, 1998.

2. Baker NA, Sept D, Joseph S, Holst MJ, and McCammon JA. Electrostatics of nanosystems: application to microtubules and the ribosome. *Proc Natl Acad Sci U S A* 98: 10037-10041, 2001.

3. Balk J, and Pilon M. Ancient and essential: the assembly of iron-sulfur clusters in plants. Trends *Plant Sci* 16: 218-226, 2011.

4. Berndt C, Hudemann C, Hanschmann EM, Axelsson R, Holmgren A, and Lillig CH. How does iron-sulfur cluster coordination regulate the activity of human glutaredoxin 2? *Antioxid Redox Signal* 9: 151-157, 2007.

5. Berriman M, Haas BJ, LoVerde PT, Wilson RA, Dillon GP, Cerqueira GC, Mashiyama ST, Al-Lazikani B, Andrade LF, Ashton PD, Aslett MA, Bartholomeu DC, Blandin G, Caffrey CR, Coghlan A, Coulson R, Day TA, Delcher A, DeMarco R, Djikeng A, Eyre T, Gamble JA, Ghedin E, Gu Y, Hertz-Fowler C, Hirai H, Hirai Y, Houston R, Ivens A, Johnston DA, Lacerda D, Macedo CD, McVeigh P, Ning Z, Oliveira G, Overington JP, Parkhill J, Pertea M, Pierce RJ, Protasio AV, Quail MA, Rajandream MA, Rogers J, Sajid M, Salzberg SL, Stanke M, Tivey AR, White O, Williams DL, Wortman J, Wu W, Zamanian M, Zerlotini A, Fraser-Liggett CM, Barrell BG, and El-Sayed NM. The genome of the blood fluke *Schistosoma mansoni*. *Nature* 460: 352-358, 2009.

6. Bonilla M, Denicola A, Marino SM, Gladyshev VN, and Salinas G. Linked

thioredoxin-glutathione systems in platyhelminth parasites: alternative pathways for glutathione reduction and deglutathionylation. *J Biol Chem* 286: 4959-4967, 2011.

7. Bonilla M, Denicola A, Novoselov SV, Turanov AA, Protasio A, Izmendi D, Gladyshev VN, and Salinas G. Platyhelminth mitochondrial and cytosolic redox homeostasis is controlled by a single thioredoxin glutathione reductase and dependent on selenium and glutathione. *J Biol Chem* 283: 17898-17907, 2008.

8. Brautigam L, Johansson C, Kubsch B, McDonough MA, Bill E, Holmgren A, and Berndt C. An unusual mode of iron-sulfur-cluster coordination in a teleost glutaredoxin. *Biochem Biophys Res Commun* 436: 491-496, 2013.

9. Carballal S, Trujillo M, Cuevasanta E, Bartesaghi S, Moller MN, Folkes LK, Garcia-Bereguiain MA, Gutierrez-Merino C, Wardman P, Denicola A, Radi R, and Alvarez B. Reactivity of hydrogen sulfide with peroxynitrite and other oxidants of biological interest. *Free Radic Biol Med* 50: 196-205, 2011.

10. Carvalho PC, Fischer JS, Xu T, Yates JR 3rd, and Barbosa VC. PatternLab: from mass spectra to label-free differential shotgun proteomics. In: *Curr Protoc Bioinformatics*. Hoboken, NJ: John Wiley & Sons, Inc., 2012, Unit13 19.

11. Collet JF, Peisach D, Bardwell JC, and Xu Z. The crystal structure of TrxA(CACA): Insights into the formation of a [2Fe-2S] iron-sulfur cluster in an Escherichia coli thioredoxin mutant. *Protein Sci* 14: 1863-1869, 2005.

12. Cunningham LJ, and Olson PD. Description of *Hymenolepis microstoma* (Nottingham strain): a classical tapeworm model for research in the genomic era. *Parasites & Vectors* 3:123-131, 2010.

13. Emsley P, Lohkamp B, Scott WG, and Cowtan K. Features and development of Coot. *Acta Crystallogr D Biol Crystallogr* 66: 486-501, 2010.

14. Fernandes AP, Fladvad M, Berndt C, Andresen C, Lillig CH, Neubauer P, Sunnerhagen M, Holmgren A, and Vlamis-Gardikas A. A novel monothiol glutaredoxin (Grx4) from *Escherichia coli* can serve as a substrate for thioredoxin reductase. *J Biol Chem* 280: 24544-24552, 2005.

15. Golinelli MP, Gagnon J, and Meyer J. Specific interaction of the [2Fe-2S] ferredoxin from *Clostridium pasteurianum* with the nitrogenase MoFe protein. *Biochemistry* 36: 11797-11803, 1997.

16. Hanschmann EM, Godoy JR, Berndt C, Hudemann C, and Lillig CH. Thioredoxins, glutaredoxins, and peroxiredoxins--molecular mechanisms and health significance: from cofactors to antioxidants to redox signaling. *Antioxid Redox Signal* 19: 1539-1605, 2013.

17. Holmgren A. Thioredoxin catalyzes the reduction of insulin disulfides by dithiothreitol and dihydrolipoamide. *J Biol Chem* 254: 9627-9632, 1979.

18. Holmgren A, and Aslund F. Glutaredoxin. *Methods Enzymol* 252: 283-292, 1995.

19. Holmgren A, Johansson C, Berndt C, Lonn ME, Hudemann C, and Lillig CH. Thiol redox control via thioredoxin and glutaredoxin systems. *Biochem Soc Trans* 33: 1375-1377, 2005.

20. Johansson C, Lillig CH, and Holmgren A. Human mitochondrial glutaredoxin reduces S-glutathionylated proteins with high affinity accepting electrons from either glutathione or thioredoxin reductase. *J Biol Chem* 279: 7537-7543, 2004.

21. Johansson C, Roos AK, Montano SJ, Sengupta R, Filippakopoulos P, Guo K, von Delft F, Holmgren A, Oppermann U, and Kavanagh KL. The crystal structure of human GLRX5: iron-sulfur cluster co-ordination, tetrameric assembly and monomer activity. *Biochem J* 433: 303-311, 2011.

22. Larkin MA, Blackshields G, Brown NP, Chenna R, McGettigan PA, McWilliam H, Valentin F, Wallace IM, Wilm A, Lopez R, Thompson JD, Gibson TJ, and Higgins DG. Clustal W and Clustal X version 2.0. *Bioinformatics* 23: 2947-2948, 2007.

23. Lill R. Function and biogenesis of iron-sulphur proteins. *Nature* 460: 831-838, 2009.

24. Lill R, Hoffmann B, Molik S, Pierik AJ, Rietzschel N, Stehling O, Uzarska MA, Webert H, Wilbrecht C, and Muhlenhoff U. The role of mitochondria in cellular iron-sulfur protein biogenesis and iron metabolism. *Biochim Biophys Acta* 1823: 1491-1508, 2012.

25. Lill R, Srinivasan V, and Muhlenhoff U. The role of mitochondria in cytosolic-nuclear iron-sulfur protein biogenesis and in cellular iron regulation. *Curr Opin Microbiol* 22: 111-119, 2014.

26. Lillig CH, Berndt C, and Holmgren A. Glutaredoxin systems. *Biochim Biophys Acta* 1780: 1304-1317, 2008.

27. Masip L, Pan JL, Haldar S, Penner-Hahn JE, DeLisa MP, Georgiou G, Bardwell JC, and Collet JF. An engineered pathway for the formation of protein disulfide bonds. *Science* 303: 1185-1189, 2004.

28. Massey V. Studies on succinic dehydrogenase. VII. Valency state of the iron in beef heart succinic dehydrogenase. *J Biol Chem* 229: 763-770, 1957.

29. Meyer J. Ferredoxins of the third kind. *FEBS Lett* 509: 1-5, 2001.

30. Molina MM, Belli G, de la Torre MA, Rodriguez-Manzaneque MT, and Herrero E. Nuclear monothiol glutaredoxins of *Saccharomyces cerevisiae* can function as mitochondrial glutaredoxins. *J Biol Chem* 279: 51923-51930, 2004.

31. Molina-Navarro MM, Casas C, Piedrafita L, Belli G, and Herrero E. Prokaryotic and eukaryotic monothiol glutaredoxins are able to perform the functions of Grx5 in the

biogenesis of Fe/S clusters in yeast mitochondria. *FEBS Lett* 580: 2273-2280, 2006.

32. Morgan B, Ezerina D, Amoako TN, Riemer J, Seedorf M, and Dick TP. Multiple glutathione disulfide removal pathways mediate cytosolic redox homeostasis. *Nat Chem Biol* 9: 119-125, 2013.

33. Nordberg J, and Arner ES. Reactive oxygen species, antioxidants, and the mammalian thioredoxin system. *Free Radic Biol Med* 31: 1287-1312, 2001.

34. Pader I, Sengupta R, Cebula M, Xu J, Lundberg JO, Holmgren A, Johansson K, and Arner ES. Thioredoxin-related protein of 14 kDa is an efficient L-cystine reductase and S-denitrosylase. *Proc Natl Acad Sci U S A* 111: 6964-6969, 2014.

35. Pan JL, and Bardwell JC. The origami of thioredoxin-like folds. *Protein Sci* 15: 2217-2227, 2006.

36. Robinson JB, Jr., Brent LG, Sumegi B, Srere PA. An enzymatic approach to the study of the Krebs tricarboxylic acid cycle. In: *Mitochondria: A Practical Approach*, edited by Darley-Usmar VM, Rickwood D, and Wilson MT. Washington, DC: IRL Press, 1987, pp. 153–169.

37. Rodriguez-Manzaneque MT, Tamarit J, Belli G, Ros J, and Herrero E. Grx5 is a mitochondrial glutaredoxin required for the activity of iron/sulfur enzymes. *Mol Biol Cell* 13: 1109-1121, 2002.

38. Rouault TA. Biogenesis of iron-sulfur clusters in mammalian cells: new insights and relevance to human disease. *Dis Model Mech* 5: 155-164, 2012.

39. Sambrook J, Fritsch EF, and Maniatis T (Eds). *Molecular Cloning: A Laboratory Manual*, Cold Spring Harbor, NY: Cold Spring Harbor Laboratory, 1989, p. 1659.

40. Shin M. Ferredoxin-NADP reductase from spinach. *Meth Enzymol* 23: 440–447, 1971.

41. Siegel LM. A direct microdetermination for sulfide. *Anal Biochem* 11: 126-132, 1965.

42. Soding J. Protein homology detection by HMM-HMM comparison. *Bioinformatics* 21: 951-960, 2005.

43. Srinivasan V, Pierik AJ, and Lill R. Crystal structures of nucleotide-free and glutathione-bound mitochondrial ABC transporter Atm1. *Science* 343: 1137-1140, 2014.

44. Stroher E, and Millar AH. The biological roles of glutaredoxins. *Biochem J* 446: 333-348, 2012.

45. Sturm N, Jortzik E, Mailu BM, Koncarevic S, Deponte M, Forchhammer K, Rahlfs S, and Becker K. Identification of proteins targeted by the thioredoxin superfamily in *Plasmodium falciparum*. PLoS Pathog 5: e1000383, 2009.

46. Su D, Berndt C, Fomenko DE, Holmgren A, and Gladyshev VN. A conserved cis-proline precludes metal binding by the active site thiolates in members of the thioredoxin family of proteins. *Biochemistry* 46: 6903-6910, 2007.

47. Tamarit J, Belli G, Cabiscol E, Herrero E, and Ros J. Biochemical characterization of yeast mitochondrial Grx5 monothiol glutaredoxin. *J Biol Chem* 278: 25745-51, 2003.

48. Tamura K, Stecher G, Peterson D, Filipski A, and Kumar S. MEGA6: Molecular Evolutionary Genetics Analysis version 6.0. *Mol Biol Evol* 30: 2725-2729, 2013.

49. Tsai IJ, Zarowiecki M, Holroyd N, Garciarrubio A, Sanchez-Flores A, Brooks KL, Tracey A, Bobes RJ, Fragoso G, Sciutto E, Aslett M, Beasley H, Bennett HM, Cai J, Camicia F, Clark R, Cucher M, De Silva N, Day TA, Deplazes P, Estrada K, Fernandez C, Holland PW, Hou J, Hu S, Huckvale T, Hung SS, Kamenetzky L, Keane JA, Kiss F, Koziol U, Lambert O, Liu K, Luo X, Luo Y, Macchiaroli N, Nichol S, Paps J, Parkinson J,

Pouchkina-Stantcheva N, Riddiford N, Rosenzvit M, Salinas G, Wasmuth JD, Zamanian M, Zheng Y, Cai X, Soberon X, Olson PD, Laclette JP, Brehm K, and Berriman M. The genomes of four tapeworm species reveal adaptations to parasitism. *Nature* 496: 57-63, 2013.

50. Webb B, and Sali A. Comparative Protein Structure Modeling Using MODELLER. *Curr Protoc Bioinformatics* 47: 5.6.1-5.6.32, 2014.

51. Williams DL, Bonilla M, Gladyshev VN, and Salinas G. Thioredoxin glutathione reductase-dependent redox networks in platyhelminth parasites. *Antioxid Redox Signal* 19: 735-745, 2013.

52. Yeh AP, Chatelet C, Soltis SM, Kuhn P, Meyer J, and Rees DC. Structure of a thioredoxin-like [2Fe-2S] ferredoxin from *Aquifex aeolicus*. *J Mol Biol* 300: 587-595, 2000.

53. Zaffagnini M, Michelet L, Massot V, Trost P, and Lemaire SD. Biochemical characterization of glutaredoxins from *Chlamydomonas reinhardtii* reveals the unique properties of a chloroplastic CGFS-type glutaredoxin. *J Biol Chem* 283: 8868-8876, 2008.

54. Zhang B, Bandyopadhyay S, Shakamuri P, Naik SG, Huynh BH, Couturier J, Rouhier N, and Johnson MK. Monothiol glutaredoxins can bind linear $[Fe_3S_4]^+$ and $[Fe_4S_4]^{2+}$ clusters in addition to $[Fe_2S_2]^{2+}$ clusters: spectroscopic characterization and functional implications. *J Am Chem Soc* 135: 15153-15164, 2013.

55. Zheng H, Zhang W, Zhang L, Zhang Z, Li J, Lu G, Zhu Y, Wang Y, Huang Y, Liu J, Kang H, Chen J, Wang L, Chen A, Yu S, Gao Z, Jin L, Gu W, Wang Z, Zhao L, Shi B, Wen H, Lin R, Jones MK, Brejova B, Vinar T, Zhao G, McManus DP, Chen Z, Zhou Y, and Wang S. The genome of the hydatid tapeworm *Echinococcus granulosus*. *Nat Genet* 45:

1168-1175, 2013.

Figure legends

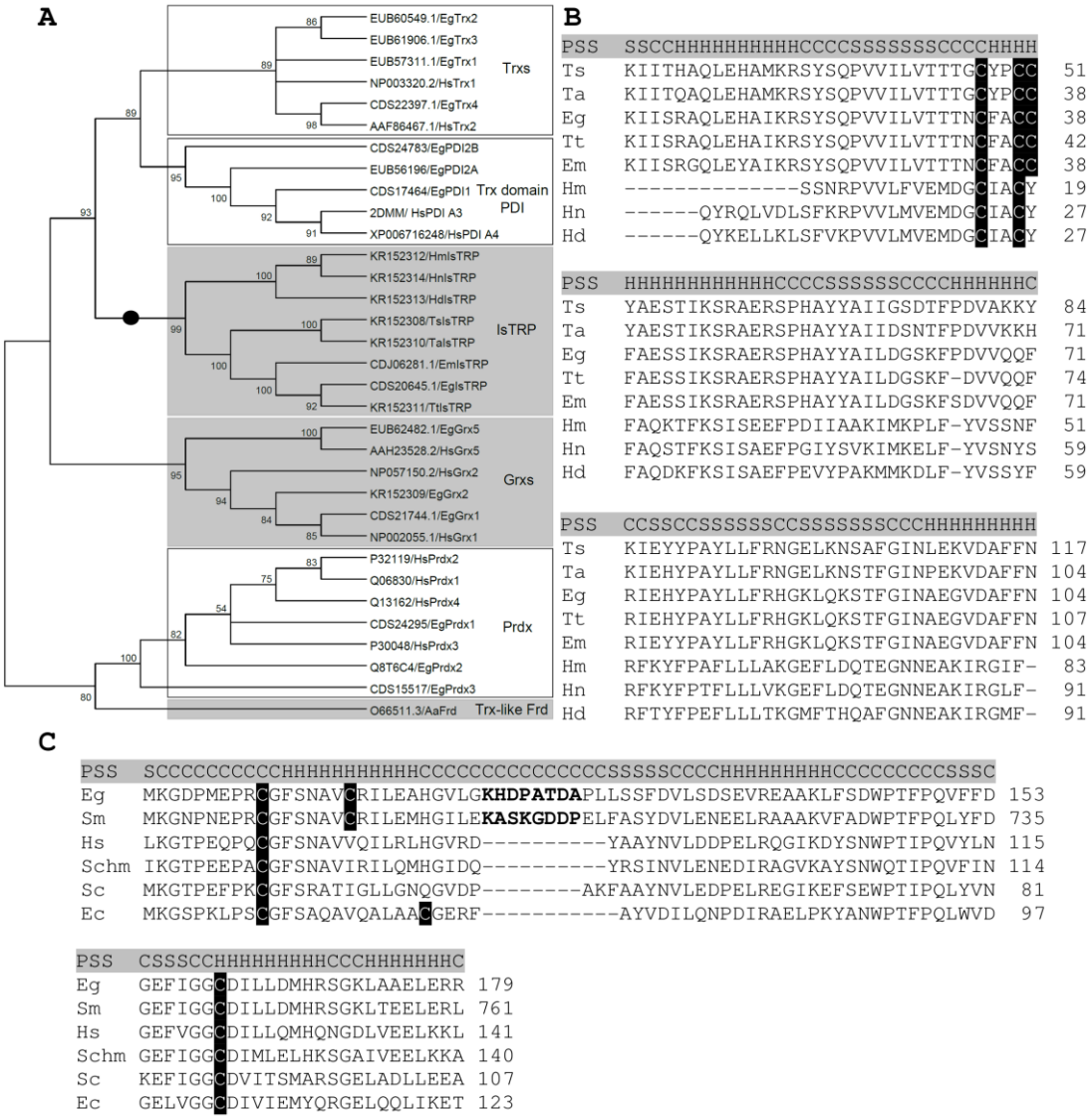

Figure 1. IsTRP and Grx5 alignment and phylogenetic analysis. A. Simplified unrooted neighbour-joining phylogeny of some Trx superfamily members (Trxs: thioredoxins,

Trx-domain of PDI: thioredoxin domain of protein disulfide isomerases, IsTRP: Iron sulfur thioredoxin-related protein, Grxs: glutaredoxins, Prdxs: peroxiredoxins, Trx-like Frd: thioredoxin-like ferredoxin). Bootstrap values were calculated using 500 iterations. The members of the Trx fold that can coordinate Fe/S are shown in grey boxes (for IsTRP, the evidence stems from this work). Sequences specific of the *Cyclophyllidea* order within the class *Cestoda* are pointed with a black circle on the branches. B and C. Protein sequence alignment of IsTRP and Grx5 ortholog proteins, respectively. Cysteine residues are highlighted in black. The residues of the insertion of tapeworm Grx5 are bolded. Predicted secondary structure (PSS) elements (highlighted in gray) are represented with (H) when it is α-helix, (S) when it is β-sheet and (C) when it is coiled. Ts. *Taenia solium* (IsTRP KR152308). Ta. *Taenia asiatica* (IsTRP KR152310). Eg. *Echinococcus granulosus* (IsTRP CDS20645, Grx5 EUB62482). Tt. *Taenia taeniformis* (IsTRP KR152311). Em. *Echinococcus multilocularis* (IsTRP CDJ06281). Hm. *Hymenolepis microstoma* (IsTRP KR152312). Hn. *Hymenolepis nana* (IsTRP KR152314). Hd. *Hymenolepis diminuta* (IsTRP KR152313). Sm. *Schistosoma mansoni* (Grx5 CCD60523). Hs. *Homo sapiens* (Grx5 AAH23528). Schm. *Schmidtea mediterranea*. Sc. *Saccharomyces cerevisiae* (Grx5 3GX8). Ec. *Escherichia coli* (Grx5 2WCI).

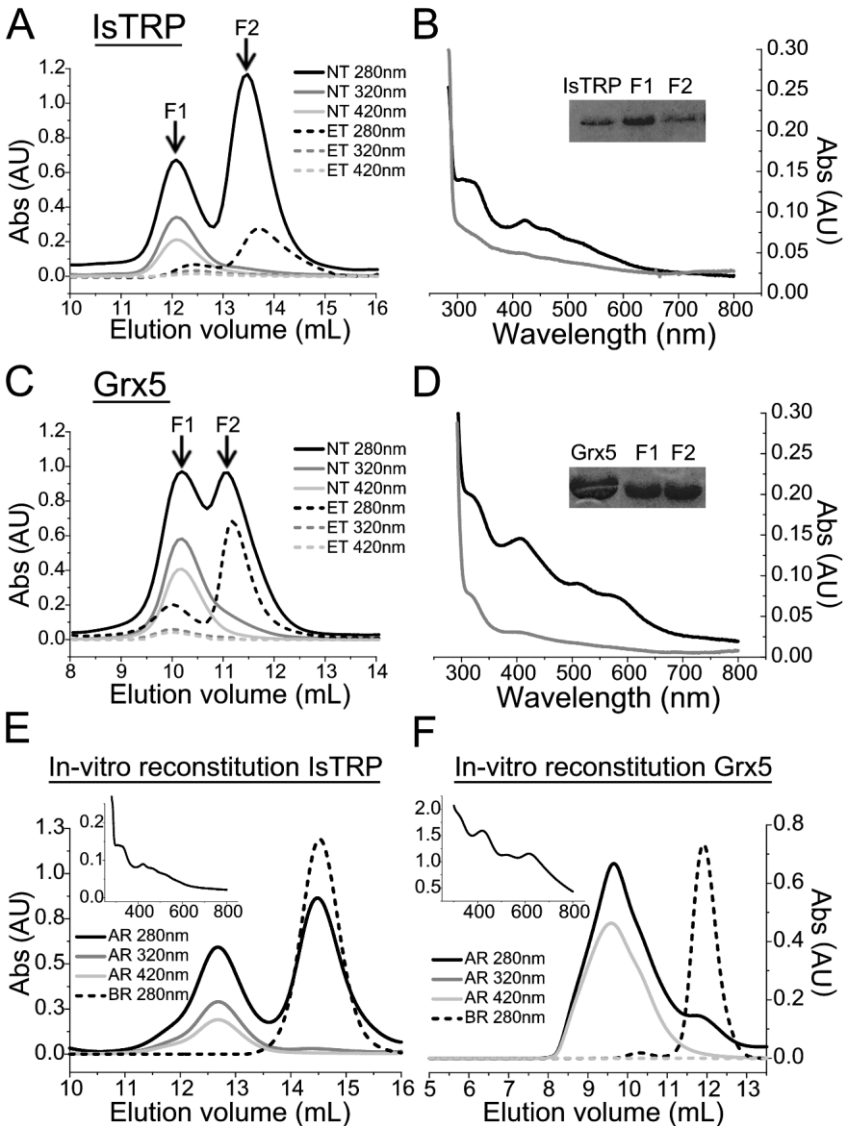

Figure 2. SEC and spectroscopic analysis of *E. granulosus* IsTRP and Grx5. Size exclusion chromatography analysis of IsTRP and Grx5 are shown in A and C respectively and were performed on a Superdex 75 10/300 GL column. Absorbance at 280 nm, 320 nm and 420 nm is shown for EDTA-treated (ET) and non-treated (NT) samples. The UV-visible spectra and SDS-PAGE of fractions F1 (black) and F2 (gray) of the untreated samples are shown for IsTRP and Grx5 in B and D respectively. SDS-PAGE of recombinant proteins prior (left lane) and after (right lane) gel filtration are shown as an inset. E and F. Size exclusion chromatography of Fe/S reconstitution mixture for

tag-free IsTRP and Grx5, respectively. Absorbance of the proteins after reconstitution (AR) and before reconstitution (BR) is shown. The spectra of the reconstituted proteins are shown in an inset.

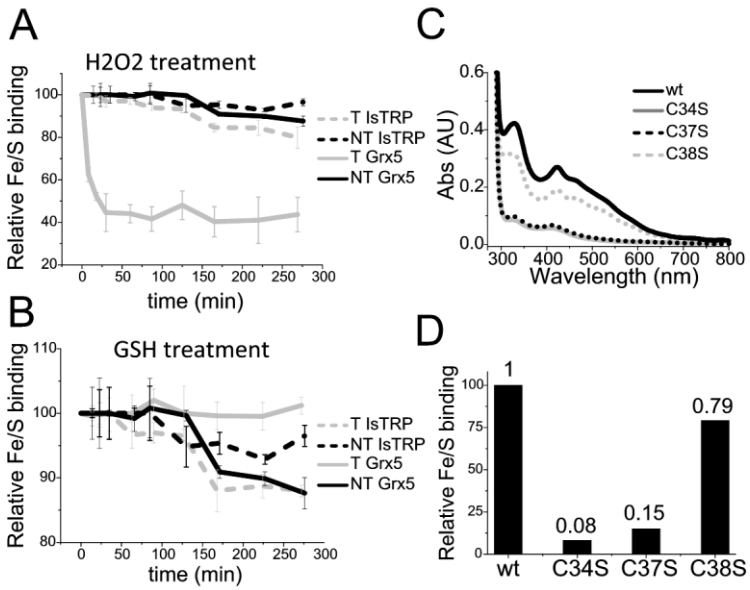

Figure 3. IsTRP and Grx5 Fe/S binding properties. A and B. Kinetics for the disassembly of holo-IsTRP and holo-Grx5 (NT) and upon treatment (T) with 10 mM of H_2O_2 or 3 mM of GSH. The loss of the Fe/S was recorded by following the decrease in absorbance at 320 nm. Error bars correspond to standard deviations of three replicates. C and D. The Fe/S coordination ability of wild type, Cys38Ser, Cys37Ser and Cys34Ser mutants was analyzed by measuring the absorbance at 320 nm of the copurified holo-proteins. Protein concetration were between 300 and 200 µM. A representative UV-visible spectrum (normalized to protein concentration) of each protein species is shown in C and the corresponding 320 nm/280 nm ratio relative to the binding of the wild type protein is shown in D.

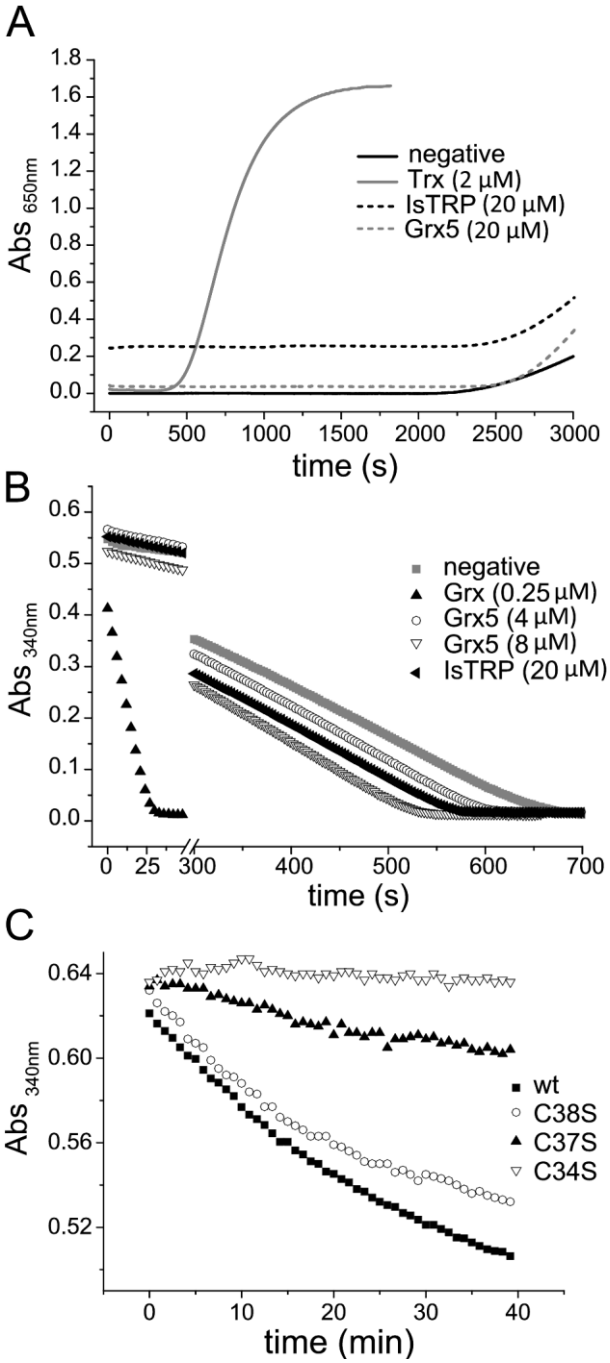

Figure 4. Activities of IsTRP and Grx5. A. Insulin reduction by dithiothreitol. 20 μM of IsTRP and Grx5; and 2 μM of a Trx from *E. granulosus*. The absorbance at 650 nm is plotted against time. B. HED activity assay. The capacity of IsTRP, Grx5 and a Grx from *E. granulosus* to deglutathionylate was evaluated. NADPH oxidation was followed by measuring absorbance at 340 nm. The full time courses obtained are shown. C.

Reduction of 20 µM wild type IsTRP (black) and mutants Cys to Ser by the TGRC31S (a TGR mutant that conserves full thioredoxin reductase activity but lacks gutathione reductase activity). 125 nM of TGR_{C31S} was used for the assay. Representative full time courses of NADPH oxidation are shown.

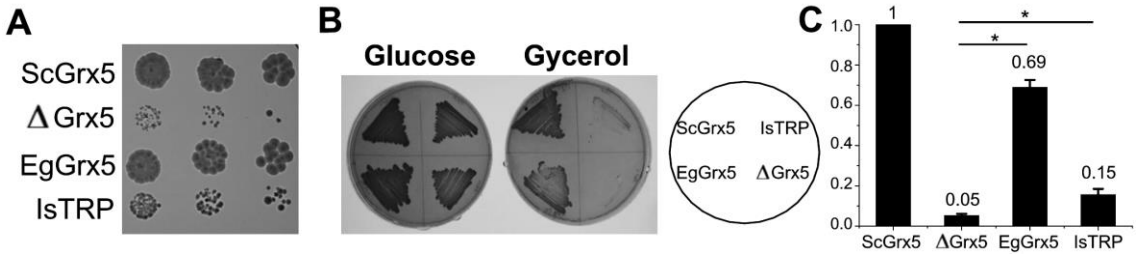

Figure 5. Rescue of the *ΔGrx5* mutant defects by Grx5 and IsTRP. A. Growth plates after 3 day-incubation at 30ºC on YPD. From left to right 1:5 serial dilutions of exponential cultures were spotted. B. Growth on YPD or YPG plates after 3 days at 30ºC. *S. cerevisiae* Grx5 (ScGrx5), *E. granulosus* (EgGrx5), *E. granulosus* IsTRP (IsTRP) and null mutant (ΔGrx5) are shown. C. Ratio between the Fe/S containing enzyme aconitase and the non-Fe/S containing enzyme malate dehydrogenase activities in exponential cultures at 30ºC in YPGal medium. Values were normalized with respect to strain MML240 that expresses yeast Grx5-HA. The values are the mean of three experiments with standard deviations. Statistical analysis was performed using one-way ANOVA (p-value < 0.05).

Tables

Table 1. Concentration ratio of iron and sulfur to holo-IsTRP.

	[Fe]/[HoloProt]	[S2-]/[HoloProt]
IsTRP	0.9 ± 0.1	0.89 ± 0.07

Iron was measured using 4,7-diphenyl-1,10-phenanthroline and acid labile sulfur was measured using the methylene blue method (see methods). Concentration of holoprotein in the analyzed fraction was estimated by analytical SEC.

Table 2. Concentration ratio between low molecular weight thiols (LMWT) and GSH and apo- or holo-form of Grx5 and -IsTRP purified from *E. coli*.

	LMWT/Prot.		GSH/Prot.	
	Grx5	IsTRP	Grx5	IsTRP
holoprotein	0.51	0.01	0.43	<0.01
apoprotein	0.11	0.01	0.09	<0.01

GSH was added to all buffers during IMAC purification of both proteins and free GSH was removed afterwards by SEC.

Table 3. Transcription profiles of genes involved in the ISC and CIA assembly machinery from adult, oncosphere (Onc), protoscolex (PSC) and hydatid cyst membrane (Cyst) of *E. granulosus*.

Components of the ISC assembly machinery					
	Gene ID	RPKM*			
		Adult	Onc†	PSC†	Cyst
NFS1	CDS19765	56	33	100	52
ISD11	EUB55154	695	964	131	306
FDXR	CDS18240	13	0	36	20
FDX2	EUB56835	16	105	52	0
FXN	CDS24551	74	122	61	85
ISCU	EUB64018	444	455	91	159
GRP75‡	CDS17875	280	2170	372	610
HSC20§	CDS23455	62	0	77	18
GRPE-L1/L2	EUB64601	82	77	96	81
Grx5	EUB62482	114	0	19	65
Components of the CIA assembly machinery					
	Gene ID	RPKM*			
		Adult	Onc†	PSC†	Cyst
NUBP1	CDS22073	64	0	48	157
NUBP2	CDS21766	118	0	44	55
CIAPIN1	EUB62290	78	0	369	125
NDOR1	EUB64339	0	0	31	26
CIAO1	CDS16778	24	78	19	24

MIP18	CDS20555	50	0	11	0
Mms19	CDS16337	32	13	59	18
NARFL	CDS21645	30	0	19	39

Transcriptomic data was obtained from (55). An adapted figure from (25) illustrating Fe/S synthesis is shown in Fig. S5.

∗ Reads per kilobase per million mapped reads

† Onc and PSC were treated for activation prior to transcriptomic analysis

‡ Generic chaperone

§ Specific co-chaperone

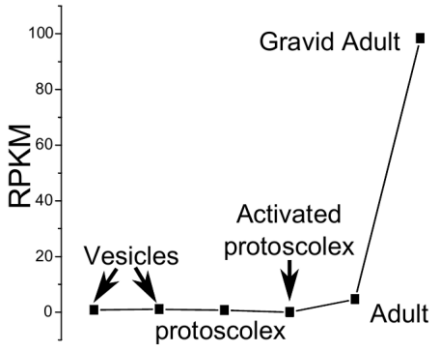

Figure S1. Transcription profiles of IsTRP from gravid adult, adult, activated protoscolex, protoscolex and vesicles of E. multilocularis. Transcriptome analysis was performed by the Parasite Genomics platform in the Wellcome Trust Sanger Institute. The data is presented as reads per kilobase per million mapped reads (RPKM).

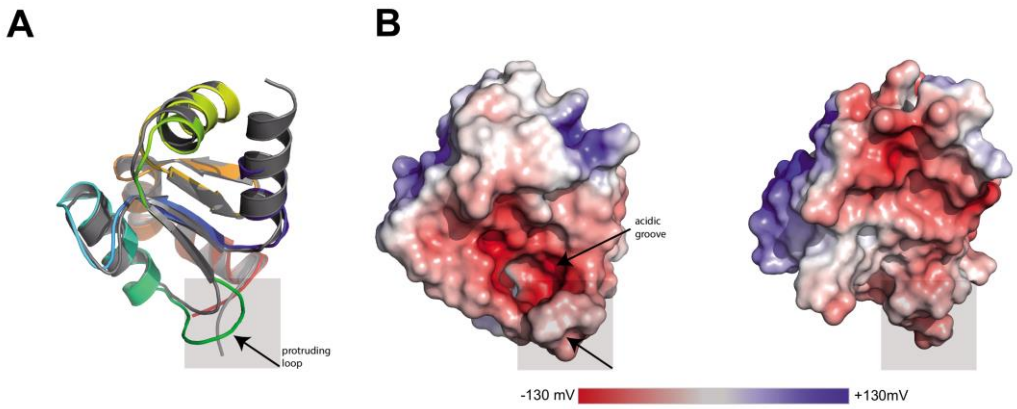

Figure S2. Structure homology comparison of Grx5 from S. cerevisiae and E. granulosus. A. Cartoon representation of a homology model for EgGrx5 3D structure. EgGrx5 is color‐coded from blue to red, for N‐terminal and C‐terminal and superposed to yeast Grx5 (gray cartoon; PDB access code: 3gx8). The extended loop discussed in the text is pointed by an arrow within a shaded square and has multiple possible conformations (an average loop is depicted, green region). B. van der Waals representation of EgGrx5 (left) and yeast Grx5 (right) monomers showing electrostatic surfaces. An acidic groove present only in EgGrx5 is indicated.

Figure S3. Full sequence of E. granulosus Grx5. The full amino acid sequence of Grx5 is shown. The sequence encoded in the expression plasmid for the recombinant protein (pH08, see table S1) is bolded. The active site is highlighted in grey and the predicted mitochondrial signal peptide (MSP) and the Grx domain are also shown.

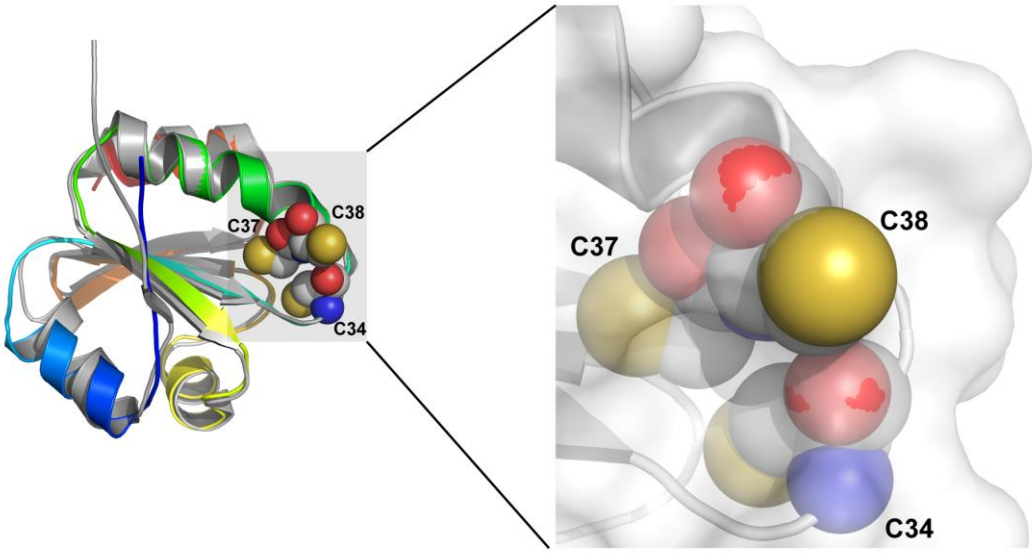

Figure S4. Structure homology comparison of IsTRP monomer with thioredoxin 1 from yeast. Cartoon representation of a homology model for IsTRP 3D structure (color‐coded from blue to red, for N‐terminal and C‐terminal) superposed to yeast thioredoxin 1 (grey cartoon; PDB access code 3f3q). The three cysteines in IsTRP are depicted as spheres. An inset of the active site is shown on the right, to provide perspective onto group orientation respect to a transparent molecular surface. Color code for spheres: orange, sulfur; white, carbon; red, oxygen; blue, nitrogen. Solvent exposure for Cys34 is variable among the models.

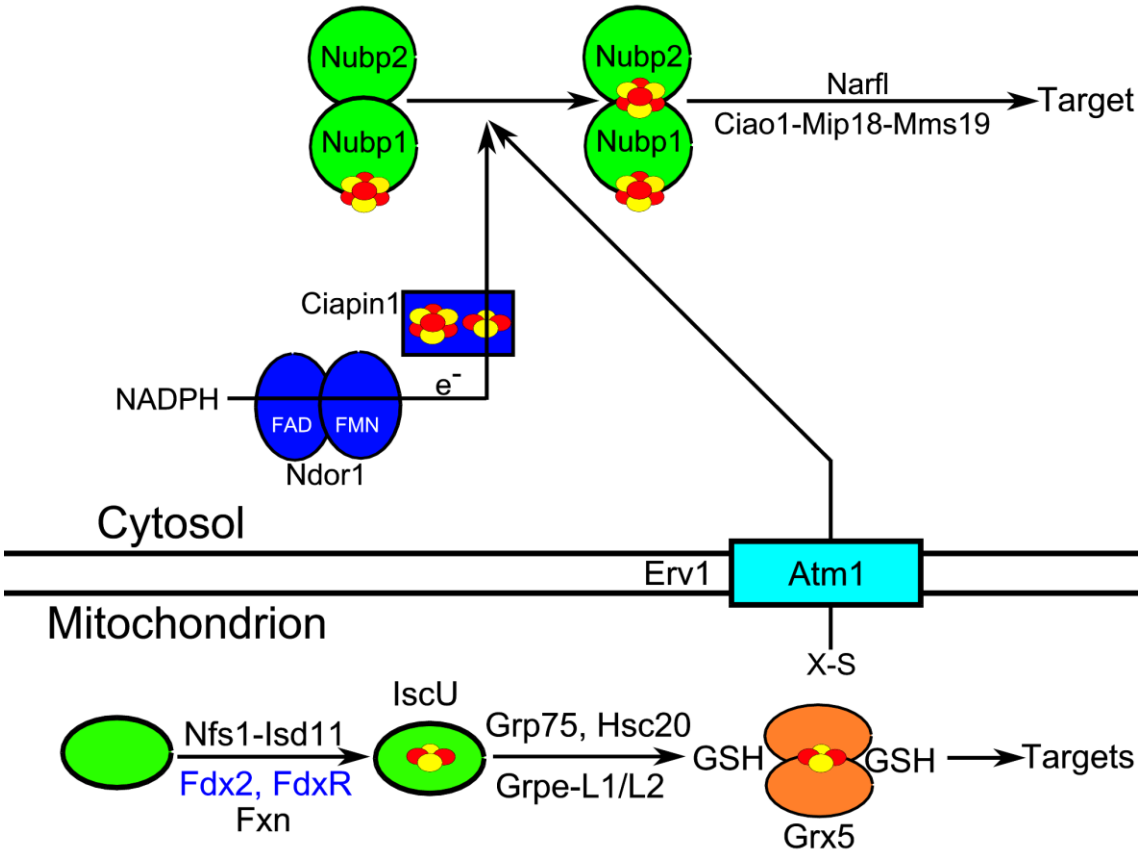

Figure S5. Illustration of Fe/S synthesis machinery in mammals. This figure was adapted from Lill, et al. 2014 (25). X-S represents the sulfur containing moiety exported from the mitochondria and sulfur and iron atoms are represented in yelow and red respectively. Scaffold proteins are shown in green and proteins involved in electron transport in blue.

Table S1. Plasmids and DNA constructs employed and generated in this work.

Construct	Vector	Eg gene	Primer pair/s	Comments
	pET28a	-	-	
	pMM221	-	-	Doxycycline controlled tTA
				transactivator, tetO2 promoter
				regions, C-terminal HA3/His6
				and MTS of S. cerevisiae Grx5
pH08	pET28a	Grx5	GGATCCACATTCGCGGCTCTACCG	Residue 43 to 194
			AAGCTTTTAATTTTTCTTCCCCTTCTC	
pH14	pET28a	IsTrx	GGATCCATGCCCGAGATTTTG	wild type
			AAGCTTTTAGAAAGAATTGAAAAAAGCG	
pH16	pET28a	IsTrx	GGATCCATGCCCGAGATTTTG	CxxSC mutant
			AAGCTTTTAGAAAGAATTGAAAAAAGCG	
			GCTTTGCATCCTGTTTTGCC	
			GGCAAAACAGGATGCAAAGC	
pH18	pET28a	IsTrx	GGATCCATGCCCGAGATTTTG	SxxCC mutant
			AAGCTTTTAGAAAGAATTGAAAAAAGCG	
			GACAAACTCCTTTGCATGCTGTTTTG	
			CAAAACAGCATGCAAAGGAGTTTGTC	
pH19	pET28a	IsTrx	GGATCCATGCCCGAGATTTTG	CxxCS mutant
			AAGCTTTTAGAAAGAATTGAAAAAAGCG	
			CTGCTTTGCATGCTCTTTTGCCGAAAG	
			CTTTCGGCAAAAGAGCATGCAAAGCAG	
pH20	pMM221	Grx5	GCGGCCGCCTGGACAAGGCGCTCCGCAAC	Residues 65 to 194
			CTGCAGATTTTTCTTCCCCTTCTCCCT	
pH21	pMM221	IsTrx	GCGGCCGCATGCCCGAGATTTTGAAAATC	Residues 1 to 106
			CTGCAGGAAAGAATTGAAAAAAGCGTC	

Restriction sites sequences are underlined.

Table S2. Yeast strains employed in this work.

Strain	Relevant phenotype	Comments/Reference
W303-1A	MATa ura3-1 ade2-1 leu2-3,112 trp1-1 his3-11,15	Wild-type
W303-1B	As W303-1A but MATα	Wild-type
MML289	MATα grx5::kanMX4	(13)
MML240	MATa grx5::kanMX4 pMM54(ScGRX5-3HA)::LEU2	(29)
pL1	MATa [pMM221::LEU2]	Integration of linear pMM221 in W303-1A
gL1	MATa [pMM221(EgGRX5-3HA)]::LEU2	Integration of linear pH20 in W303-1A
tL1	MATa [pMM221(EgGRX5-3HA)]::LEU2	Integration of linear pH21 in W303-1A
pL2	MATa grx5::kanMX4 [pMM221::LEU2]	Spore from a cross MML289XpL1
gL2	MATa grx5::kanMX4 [pMM221(EgGRX5-3HA)]::LEU2	Spore from a cross MML289XgL1
tL2	MATα grx5::kanMX4 [pMM221(EgGRX5-3HA)]::LEU2	Spore from a cross MML289XtL1